THE JOURNAL OF BIOLOGICAL CHEMISTRY VOL. 289, NO. 35, pp. 24475–24487, August 29, 2014

A Conserved Phenylalanine as a Relay between the α5 Helix and the GDP Binding Region of Heterotrimeric G_i Protein α Subunit*[S]

Received for publication, April 19, 2014, and in revised form, July 15, 2014 Published, JBC Papers in Press, July 18, 2014, DOI 10.1074/jbc.M114.572875

Ali I. Kaya[‡], Alyssa D. Lokits[§], James A. Gilbert[‡], Tina M. Iverson[‡¶], Jens Meiler[‡‖], and Heidi E. Hamm[‡1]

From the Departments of [‡]Pharmacology, [§]Neuroscience, [¶]Biochemistry, and [‖]Chemistry, Vanderbilt University Medical Center, Nashville, Tennessee 37232

Background: GPCRs regulate heterotrimeric G protein activation. However, the intermediate steps regulating GDP release are still unknown.
Results: Energy analysis pinpoints information flow through Gα-receptor interaction and GDP release.
Conclusion: Hydrophobic interactions around α5 helix, β2-β3 strands, and α1 helix are key for GDP stability.
Significance: G protein activation defines regulation of high affinity receptor interactions and plays a role defining different cellular responses.

G protein activation by G protein-coupled receptors is one of the critical steps for many cellular signal transduction pathways. Previously, we and other groups reported that the α5 helix in the G protein α subunit plays a major role during this activation process. However, the precise signaling pathway between the α5 helix and the guanosine diphosphate (GDP) binding pocket remains elusive. Here, using structural, biochemical, and computational techniques, we probed different residues around the α5 helix for their role in signaling. Our data showed that perturbing the Phe-336 residue disturbs hydrophobic interactions with the β2-β3 strands and α1 helix, leading to high basal nucleotide exchange. However, mutations in β strands β5 and β6 do not perturb G protein activation. We have highlighted critical residues that leverage Phe-336 as a relay. Conformational changes are transmitted starting from Phe-336 via β2-β3/α1 to Switch I and the phosphate binding loop, decreasing the stability of the GDP binding pocket and triggering nucleotide release. When the α1 and α5 helices were cross-linked, inhibiting the receptor-mediated displacement of the C-terminal α5 helix, mutation of Phe-336 still leads to high basal exchange rates. This suggests that unlike receptor-mediated activation, helix 5 rotation and translocation are not necessary for GDP release from the α subunit. Rather, destabilization of the backdoor region of the Gα subunit is sufficient for triggering the activation process.

Heterotrimeric G proteins play a critical role as molecular switch proteins that couple the activation of cell surface receptors, G protein-coupled receptors (GPCRs),[2] to different intracellular effector proteins mediating intracellular responses. Therefore, G proteins have a crucial role in defining the specificity and temporal characteristics of many different cellular responses (1–5).

Several structural and biophysical studies have proposed the conformation of the receptor in its active state and have identified potential receptor-mediated mechanisms for G protein activation and GDP release (6–16). Two well studied receptor-mediated G protein activation routes have been hypothesized. In the first, the binding of the GPCR to the C terminus of Gα is thought to trigger conformational changes that can be transmitted via rotation of the α5 helix of Gα to the β6-α5 turn on the purine ring of the GDP (Fig. 1) (3, 9, 17–19). In the second proposed mechanism, the GPCR is thought to take advantage of Gβγ as a nucleotide exchange factor to disrupt the phosphate interactions of the nucleotide binding pocket via destabilization of switch I-II regions through perturbing α5 interaction with the β2-β3 strands (Fig. 1) (20–25).

In 2011, Kobilka and co-workers (18) provided an important missing piece of the puzzle in the receptor-mediated G protein activation cycle by determining the structure of the β_2-adrenergic receptor-G_s heterotrimer complex structure. This groundbreaking study detailed the receptor-G protein interaction and G protein activation. This structure represents the end point in the signal transduction step. The signaling route by which an active receptor interacts with an inactive G protein and causes conformational changes that lead to the final high affinity complex of a receptor with its cognate G protein and GDP release is still unknown.

To address the conformational dynamics underlying nucleotide release from the Gα subunit, we recently generated a pre-

* This work was supported, in whole or in part, by National Institutes of Health Grants EY006062 (to H. E. H.); GM095633 (to T. M. I.); GM080403, MH090192, GM099842, and DK097376 (to J. M.); and S10 RR026915 (to Vanderbilt Robotic Crystallization Facility). This work was also supported by National Institutes of Science Grants BIO Career 0742762 and CHE 1305874 (to J. M.), U.S. Department of Energy Contract DE-AC02-06CH11357, funds from the Michigan Economic Development Corporation, and Michigan Technology Tri-Corridor Grant 085P1000817.
[S] This article contains supplemental Table S1 and Movies S1–S4.
The atomic coordinates and structure factors (codes 4PAN, 4PAM, 4PAO, and 4PAQ) have been deposited in the Protein Data Bank (http://wwpdb.org/).
[1] To whom correspondence should be addressed: Dept. of Pharmacology; 442 Robinson Research Bldg.; Vanderbilt University Medical Center, Nashville, TN 37232-6600. Tel.: 615-343-3533; Fax: 615-343-1084; E-mail: Heidi.hamm@vanderbilt.edu.

[2] The abbreviations used are: GPCR, G protein-coupled receptor; GDP, guanosine diphosphate; GTPγS, guanosine 5′-[γ-thio]triphosphate; $G\alpha_{i1}$ HI, $G\alpha_{i1}$ Hexa I; REU, Rosetta energy unit(s); EPPS, 4-(2-hydroxyethyl)-1-piperazinepropanesulfonic acid.

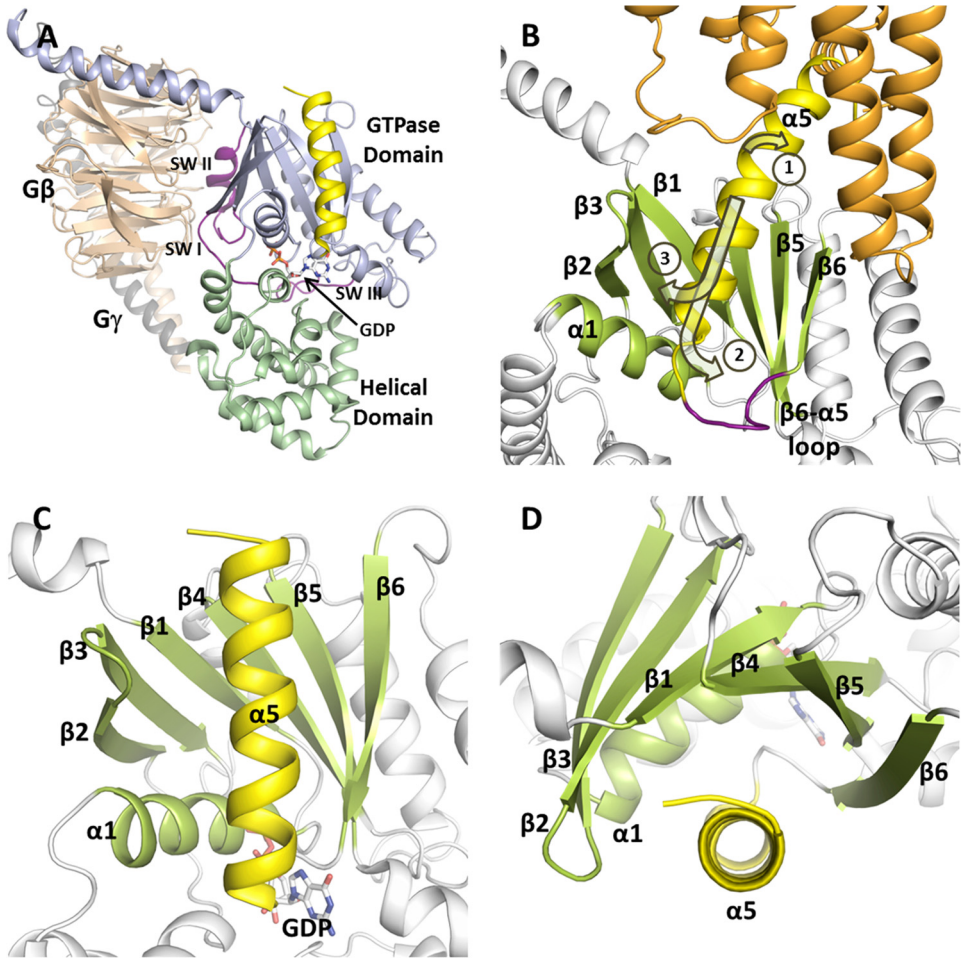

FIGURE 1. **Heterotrimeric G protein; localization and function α5 helix in G proteins.** *A*, ribbon model of heterotrimeric G protein ($G_i\alpha\beta\gamma$, Protein Data Bank entry 1GP2). The Gα subunit is composed of nucleotide binding (GTPase domain, *light blue*) and helical domains (*green*). The α5 helix and switch (*SW*) regions are colored *yellow* and *purple*, respectively. GDP is shown as *sticks*. *B*, receptor-mediated (*orange*) G protein activation routes. The binding of the GPCR to the C terminus of Gα is thought to trigger conformational changes that can be transmitted via rotation of the α5 helix (*black*, *arrow 1*) of Gα to the β6-α5 loop (*purple*, *arrow 2*) that binds the purine ring of the GDP. In the second route, disruption of the phosphate interactions with the nucleotide binding pocket via destabilization of switch I-II regions through perturbing α5 interaction with the β2-β3 strands (*arrow 3*). The rhodopsin-G_i complex model adapted from Alexander *et al.* (26). *C* and *D*, the α5 helix is one of the most critical regions for G protein stability and activation. *A* and *B*, the α5 helix (*yellow*) is protected by six β strands (β1–β6) and one α helix (α1) (*green*). The structure is adapted from the crystal structure of the G_i heterotrimer (Protein Data Bank entry 1GP2).

dictive computational model of the energy of receptor activation with the goal of understanding conformational changes and connections between potential key residues during G protein activation (26). In this model of the rhodopsin-$G_i\alpha\beta\gamma$ complex, it was suggested that the α5 helix is the most critical region for G protein stability and activation and is consistent with previous studies (9, 12, 14, 15, 27). The α5 helix is protected and surrounded with primarily hydrophobic interactions within six β strands (β1–β6) and one α helix (α1) (Fig. 1, *C* and *D*). Energetic analysis predicted that residues Phe-191 and Phe-196 in β2-β3, Ile-265 and Phe-267 in β5, Tyr-320 and His-322 in β6 strands, and Gln-52 and Met-53 in the α1 helix are making critical interactions with the α5 helix in both basal and receptor-mediated G protein activation (26). These key residues might either be important for the overall structural integrity of the GTPase domain during the activation process, or they may be directly involved in activation.

To identify the residue-residue interactions that are critical for activation as a part the signaling pathway, we systematically tested the effects of these residue-residue interactions on G protein activation. The residues were examined using biochemical, computational, and structural approaches in both basal and receptor-bound states. In this study, recombinant $G\alpha_{i1}$ was used for all experiments instead of visual G protein, given that $G\alpha_i$ is a very close homolog of $G\alpha_t$ yet much more easily expressed in *Escherichia coli*. Our data showed that single mutations in the β5 and β6 strands that face the α5 helix were not able to break hydrophobic interactions and trigger GDP release from G protein in both receptor-bound and unbound states. In the receptor-bound state, using pairwise coupling energy analysis, we predicted that the α5 rotation compensates the effect of β5-β6 mutations on protein activation.

However, the hydrophobic interactions on the opposite side of the α5 helix were predicted to directly affect G protein function. Energetic analysis predicted that Phe-336 is the most critical residue in the α5 helix; it creates a hydrophobic hot spot of G protein activation, consistent with previous studies (14, 28, 29). The amplitude of this effect was correlated with decreasing hydrophobicity of the side chain. Experimentally tracing the hydrophobic interactions around the Phe-336 residue together

with computational analysis provided evidence for a dynamic interplay between Phe-336, the β2 and β3 strands, and the α1 helix on the G protein activation route.

EXPERIMENTAL PROCEDURES

Materials—The TSKgel G2000SW column, GDP, and GTPγS were purchased from Sigma. All other reagents and chemicals were of the highest available purity.

Rosetta Interface Energy Calculations—Interface energies were computed following the Rosetta ΔΔ*G* protocol previously described (26). Briefly, we leveraged the previously published ensembles of 10 structures of the G protein in the basal state and receptor-bound state. Residue-residue interactions across α1 helix/GTPase domain interface were evaluated by measuring energetic perturbations when computationally removing the α1 helices from the models. The α1 helix was defined as residues 45–58. For all analyses, GDP remained fixed within the nucleotide binding pocket. The ΔΔ*G* value is reported as an average over the 10 structural models in Rosetta energy units (REU). Absolute values larger than 0.5 REU are considered to be significant. Using the standard deviation over the 10 structures, a Z-score was computed. The total ΔΔ*G* value across the interface is calculated as the sum of individual residue contributions.

Rosetta Pairwise Binding Energy Calculations—Average energies between pairwise interacting residues were computed using Rosetta's per residue energy breakdown protocol. The energy between all possible pairs of interacting amino acid residues within the G protein were calculated across the previously published ensembles of 10 structures (26). These energies between all residues pairs were then averaged across the 10 models in both the receptor-bound and basal state. Predicted energy values are reported in REU and considered significant if greater than 0.5 REU.

Preparation of Urea Washed Rod Outer Segment Membranes and $G\beta_1\gamma_1$—Urea washed rod outer segment membranes and $G\beta_1\gamma_1$ were prepared from bovine retina as described previously (30, 31).

Construction, Expression, and Purification of Proteins—Briefly, the pSV277 expression vector encoding $G\alpha_{i1}$ with N-terminal His tag served as the template for introducing individual mutant substitutions using the QuikChange system (Stratagene). All mutations were confirmed by DNA sequencing (DNA Sequencing Facility, Vanderbilt University). The mutant constructs were then expressed and purified as previously described (32). The purified proteins were cleaved with thrombin (Sigma; final concentration, 0.5 unit/mg) for 16 h at 4 °C to remove the N-terminal His tag. The sample was then loaded onto a nickel-nitrilotriacetic acid column to separate the protein from the cleaved His tag and any uncleaved fraction. For further purification, the protein solution was loaded onto a size exclusion column (TSKgel G2000SW) that was equilibrated in buffer A (50 mM Tris-HCl, pH 7.4, 150 mM NaCl, 2 mM $MgCl_2$, 40 μM GDP (or 1 μM GTPγS), 2 mM DTT, and 100 μM PMSF). SDS-PAGE was used to test the purity of the proteins. Protein concentrations were determined by Bradford assay (33).

Nucleotide Exchange Assay—The basal rate of GTPγS binding was determined by monitoring the relative increase in the intrinsic tryptophan (Trp-211) fluorescence (λex 290 nm, λem 340 nm) of $G\alpha_{i1}$ (200 nM) in buffer containing 50 mM Tris (pH 7.2), 100 mM NaCl, and different amounts of $MgCl_2$ for 60 min at 25 °C after the addition of 10 mM GTPγS. Receptor-mediated nucleotide exchange was determined with $G\beta1\gamma1$ (400 nM) in the presence of 50 nM rhodopsin at 21 °C for 60 min after the addition of GTPγS. The data were normalized to the baseline and maximum fluorescence and then fit to the exponential association equation ($Y = Y_{max} * (1 - e^{-kt})$), to calculate the rate constant (k) as previously described (9).

Intrinsic Trp Fluorescence Assay with AlF—Intrinsic tryptophan (Trp-211) fluorescence upon AlF_4^- activation, relative to emission in the GDP bound state of G protein α subunit, was monitored as previously described (34). The data represent the averages from six to eight experiments.

Trypsin Digestion and Analysis—2 μg of $G\alpha_{i1}$ were incubated in buffer containing 50 mM Tris (pH 7.5), 100 mM NaCl, 20 μM GDP, and different amounts of $MgCl_2$ (0.5, 1, and 2 mM). 10 mM NaF and 50 μM $AlCl_3$ were added to samples and then incubated for 2 min at 25 °C. One microliter of a 1 mg/ml TPCK trypsin solution was added and incubated on ice for 25 min. The reaction was stopped by adding 2.5 μl of termination solution (10 mg/ml aprotinin, 10 mM PMSF). Subsequently, samples were boiled with Laemmli sample buffer for 5 min and run on a 12.5% SDS-polyacrylamide gel, stained with Coomassie Blue, and quantified by densitometry (Multimager; Bio-Rad) (30, 35, 36).

Cross-linking—An expression vector encoding $G\alpha_{i1}$ with six amino acid substitutions at solvent-exposed cysteines ($G\alpha_{i1}$ HI) and an internal His_6 tag between residues Met-119 and Thr-120 served as the template for introducing individual cysteine substitutions using the QuikChange system (Stratagene) as describe above. The bifunctional cross-linking reagent bismaleimidoethane (Pierce) was incubated in a 2:1 molar ratio with $G\alpha_{i1}$ HI as previously described (37). The concentrated, cross-linked monomeric protein was then purified by size exclusion chromatography on a calibrated G2000SW column. Calibration was performed under the same conditions as purification, using a broad range of molecular weight standards (Bio-Rad) (37).

Membrane Binding Assay—The ability of mutant Gα subunits to bind rhodopsin in urea-washed rod outer segment membranes was determined as previously described (9). Each sample was evaluated by comparison of the amount of $G\alpha_{i1}$ subunit within the pellet or supernatant to the total amount of $G\alpha_{i1}$ subunit in both treatments expressed as a percentage of the total $G\alpha_{i1}$ protein. The data represent the averages of three experiments.

Protein Crystallization, Data Collection, and Structure Determination—Purified GDP bound Gα subunits were exchanged into crystallization buffer (50 mM EPPS, pH 8.0, 1 mM EDTA, 2 mM $MgCl_2$, 5 mM DTT, 1 mM GDP) using a size exclusion chromatography column. The appropriate fractions were pooled as described above, and SDS-PAGE was used to assess to test the purity of the proteins. Crystals were grown by the hanging drop vapor diffusion method at 18 °C by equilibration against a reservoir solution containing 2.0–2.3 M $(NH_4)_2SO_3$ and 100 mM sodium acetate (pH 5.9–6.4). Proteins

TABLE 1
Crystallographic data collection and refinement statistics

	F336C-GDP	F336C-GTPγS	F336Y-GDP	F336Y-GTPγS
Data Collection and Processing[a]				
Beamline	21-ID-G	21-ID-G	21-ID-G	21-ID-G
Space groups	I4	$P3_221$	I4	$P3_221$
Cell dimensions				
a, *b*, *c* (Å)	121.1, 121.1, 68.18	79.2, 79.2, 107.9	121.5, 121.5, 68.2	79.3, 79.3, 105.1
α, β, γ (degrees)	90, 90, 90	90, 90, 120	90, 90, 90	90, 90, 120
Resolution (Å)	34–2.1 (2.18–2.1)	31–2.0 (2.07–2.0)	20–2.4 (2.5–2.4)	42–2.0 (2.07–2.0)
Total reflections	255,402	307,412	177,466	437,402
Unique reflections	28,903	26,186	19,617	26,483
R_{sym} (%)[b]	5.3 (37.9)	10.1 (44.7)	6.2 (32)	10.2 (44.6)
R_{pim} (%)[c]	2.9 (23.2)	5.2 (23.5)	3.3 (18.4)	4.7 (20.7)
$<I>/<\sigma>$	19.9 (2.6)	13.5 (3.1)	19.3 (3.46)	17.5 (3.9)
Completeness (%)	99.6 (99.5)	100 (100)	99.3 (99)	100 (100)
Refinement statistics				
R_{work} (%)[d]	18.8	16.4	18.2	16.9
R_{free} (%)	21.8	20.8	23.2	20.6
Root mean square deviations				
Bond (Å)	0.008	0.007	0.008	0.007
Angle (°)	1.029	0.981	1.011	1.009
Ramachandran statistics[e]				
Favored (%)	98.5	99.06	98.11	98.42
Allowed (%)	1.5	0.94	1.89	1.58
Outliers (%)	0.0	0.0	0.0	0.0

[a] Numbers in parentheses indicate statistics for the highest shell.
[b] $R_{sym} = \Sigma|I_i - \langle I \rangle|/\Sigma|I_i|$, where I is intensity, I_i is the ith measurement, and $\langle I \rangle$ is the weighted mean of I.
[c] $R_{pim} = \Sigma_{hkl}\sqrt{[1/(N-1)]}\Sigma_i|I_i(hkl) - I(hkl)|/\Sigma_{hkl}\Sigma_i I_i(hkl)$, where I is running over the number of independent observations of reflection hkl, and N is representing the number of replicate observations.
[d] $R_{work} = \Sigma||F_o| - |F_c||/\Sigma|F_o|$, where F_o and F_c are the observed and calculated structure factor amplitudes. R_{free} is the same as R_{work} for a set of data omitted from the refinement.
[e] Ramachandran analysis from MOLPROBITY (53).

(10 mg/ml) were mixed 1:2.5 ratio with reservoir solution and crystals appeared after 14–18 days with in the space group I4. A similar strategy was used to grow crystals in GTPγS bound form of $G\alpha_{i1}$ proteins. Proteins were incubated with 10 μM GTPγS for 30 min on ice and then storage buffer replaced the crystallization solution containing 50 μM GTPγS instead of GDP. $G\alpha_{i1}$-GTPγS samples crystallized in the space group $P3_221$. Crystals were cryo-protected prior to data collection by briefly soaking in stabilization solution containing 18% glycerol and 2.4 M $(NH_4)_2SO_3$ for ~30 s and cryo-cooled by immersion in liquid nitrogen.

Data sets were collected at the Life Sciences Collaborative Access Team (21-ID-G) of the Advanced Photon Source at Argonne National Laboratory at −180 °C using a wavelength of 0.98 Å on a MAR CCD detector. The data were processed and scaled using the HKL2000, CCP4, and Phenix suites (38–40). Crystallographic data processing and refinement statistics are reported in Table 1. Criteria for data cutoff were a combination of R_{sym} and I/σ, which both rose to unacceptable levels if the resolution were extended by $G_i\alpha$. The structures of the $G\alpha_{i1}$-GDP and $G\alpha_{i1}$-GTPγS complexes were determined by molecular replacement using 1GDD (WT $G\alpha_{i1}$-GDP) (41) and 1GIA ($G\alpha_{i1}$-GTPγS·Mg^{2+}) (42) as search models for Phaser-MR in the Phenix suite (40). Because 1GDD and 1GIA preceded the requirement for deposition of structural factors R_{free} reflections were randomly selected for F336C variant and was the same as F336Y. As a result, the free R is of limited utility. Model building was performed in Coot (43) using composite omit maps calculated in Phenix (40) to minimize model bias. Refinement conducted by both CNS (44) and Phenix, final refinements done by Phenix suite. In the final model, the regions corresponding to amino acids 1–8 and 203–211 in F336C-GDP and amino acids 1–8, 202–217, and 233–240 in F336Y-GDP are not included. Similarly, in the GTPγS-bound structures, amino acids 1–32 and 349–354 are not included because of lack of electron density. Structural superpositions were performed using Superpose for the Cα carbon backbone in the CCP4 suite (45, 46). All structural images were made with PyMOL (PyMOL Molecular Graphics System, version 1.5.0.4; Schrödinger) unless otherwise indicated.

RESULTS

In this study, our strategy was to test residues around the α5 helix that were previously identified as critical for the function of this helix during G protein activation. Residues were examined using biochemical, computational, and structural approaches in both basal and receptor-bound states.

The Effects of β5-β6 Strand Mutants on G Protein Activation—In our previous study, we proposed four residues that face the α5 helix in β5 (Ile-265 ands Phe-267) and β6 (Tyr-320 and His-322) (26). Any one of these might be critical for α5 helix stability and therefore the G protein activation (Fig. 2*A* and Ref. 26). To test the effect of these residues on G protein function, we evaluated nucleotide exchange rates after introduction of site-directed mutations. Basal and receptor-mediated nucleotide exchange rates of mutants were determined by monitoring the relative increase in the intrinsic tryptophan (Trp-211) fluorescence of $G\alpha_{i1}$. All of the mutants showed similar nucleotide exchange rates compare with WT $G\alpha_{i1}$ in both receptor-bound and unbound states (Fig. 2*B*). The simplest way to explain these data would be that those residues do not play a major role in G protein activation or that a single mutation is not enough to disturb the α5 helix for GDP release. However, when we computed pairwise residue interactions, we identified interesting details for receptor-mediated activation. In the basal state, Ile-265, Phe-267, Tyr-320, and His-322 were inter-

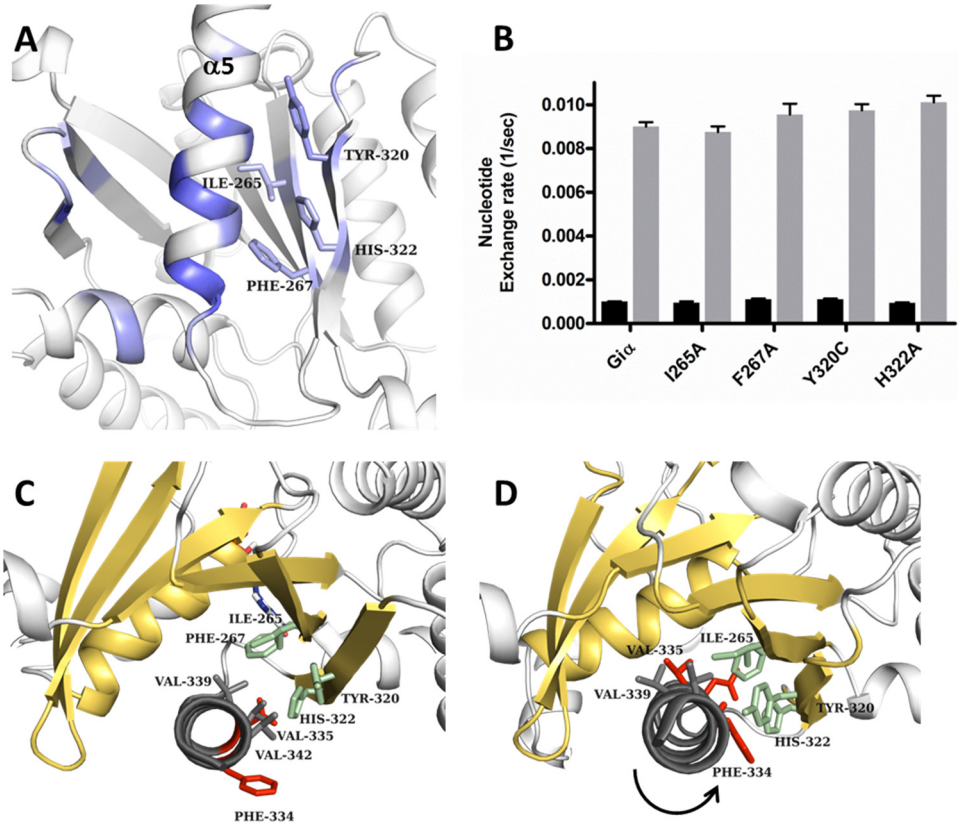

FIGURE 2. **The effects of β5-β6 strands mutations on G protein activation.** *A*, Rosetta energy analysis of the interface between the α5 helix (*black*) and the GTPase domain in the receptor-bound state. Residues are colored by the interaction energy as reported in REU (*dark blue*, the most attractive). Calculations are adapted from Ref. 26. *B*, basal (*black bars*) and receptor-mediated (*gray bars*) nucleotide exchange rates for the β5 strand (I265A and F267A) and β6 strand (Y320C and H322A) mutations in $G\alpha_{i1}$ proteins. Nucleotide exchange was monitored by measuring the enhancement in intrinsic tryptophan (Trp-211) fluorescence (excitation, 290 nm; emission, 340 nm) as a function of time after addition of GTPγS (52). *C*, most favorable interactions between the α5 helix (Val-335, Val-339, and Val-342), β5 strand (Ile-265 and Phe-267), and β6 strand (Thr-320 and His-322) interface in the basal state. *D*, after receptor interaction and α5 helix rotation (*arrow*), the same residues in β5 and β6 were hydrophobically interacting with new residues in the α5 helix (*red*). Please see supplemental Table S1 and supplemental Movies S1–S3 for full interactions in both receptor-bound and unbound states.

acting hydrophobically with Val-339, Val-335, Val-342, and Val-335, respectively, within the α5 helix. After receptor interaction and α5 helix rotation, the same residues in β5 and β6 were predicted to hydrophobically interact with new sets of residues in the α5 helix that were previously pointing toward solvent and not involved in binding in the basal state. Specifically Ile-265, Phe-267, Tyr-320, and His-322 started to interact with Ala-338, Asn-331, Ala-338, and Phe-334, respectively (Fig. 2, *C* and *D*; see supplemental Table S1 and supplemental Movies S1–S3 for full data). The α5 helix can glide along this hydrophobic surface during its rotation. These calculations thus suggested how new interactions on the rotated the α5 helix can possibly compensate for the effect of single mutations in β5 and β6 strands during receptor-mediated G protein activation.

The Effects of Phe-336 Mutants on G Protein Activation—To test the role of interactions with the opposite site of the α5 helix post-rotation, we focused on one specific residue in the α5 helix, Phe-336. Phe-336 is one of the highly conserved residues in the Gα protein family as well as the small GTPases. The side chain faces the β1, β2, and β3 strands as well as the α1 helix, which creates one of the conserved hydrophobic clusters in the Gα subunit. Our previous energetic study predicted that Phe-336 is the most critical residue for both basal and receptor-mediated G protein activation within the α5 helix (Fig. 3, *A* and *B*) (26). To test the effect of mutating this residue, we substituted Phe-336 with residues with decreasing hydrophobicity. All of the Phe-336 mutants displayed increased basal exchange rates compared with WT (Fig. 3*C*). Furthermore, a strong correlation was identified between the hydrophobicity of this residue and basal activity (Fig. 3*E*). The fastest nucleotide exchange rate was detected for F336Y. However, in receptor-mediated activation, the nucleotide exchange rates were decreased compared with WT without any correlation with hydrophobicity (Fig. 3, *D* and *F*; supplemental Movies S2 and S4). This result is consistent with a rotation of α5, leading to a new surface-exposed location of Phe-336 during α5 helix rotation and translation caused by interaction with the receptor (26). Overall, these data suggest that Phe-336 is one of the critical control points that regulate GDP release during G protein activation.

The Effects of Phe-336 Mutations on β6-α5 Loop; Cross-linking α1 and α5 Helices—The most obvious connection between the α5 helix and the nucleotide binding pocket is the β6-α5 loop. Perturbation of the α5 helix during receptor-mediated activation would disturb the interaction between the β6-α5 loop and the guanine ring of the nucleotide, leading to destabilization of the GDP in its binding pocket and domain opening of the α subunit. To test the effect of Phe-336 mutations on this

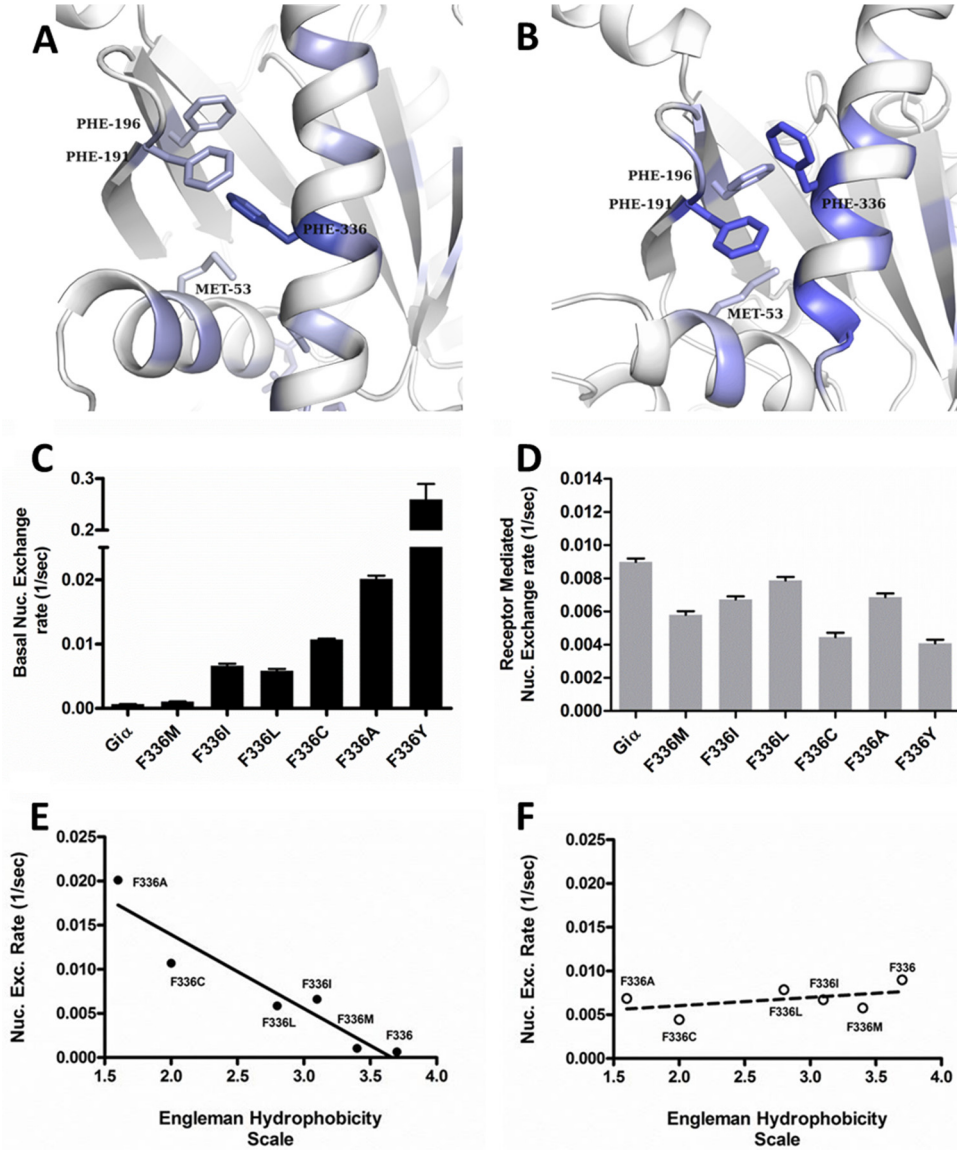

FIGURE 3. **The effect of Phe-336 residue on G protein activation.** *A* and *B*, Rosetta energy analysis of the interface between the α5 helix and GTPase domain in the basal state (*A*) and receptor-bound state (*B*). Residues are colored by the interaction energy REU (*dark blue*, the most attractive). Calculations adapted from (26). *C* and *D*, basal (*C*) and receptor-mediated (*D*) nucleotide (*Nuc.*) exchange (*Exc.*) rates of $G\alpha_{i1}$ Phe-336 mutants. The data were normalized to the baseline and maximum fluorescence and then fit to the exponential association equation ($Y = Y_{max} * (1 - e^{-kt})$) to calculate the rate constant (*k*). The data were collected at 21 °C for 60 min. The results represent the means ± S.E. values of at least three independent experiments. *E* and *F*, correlation between nucleotide exchange rates and hydrophobicity identity of the amino acids in basal (*E*) and receptor-bound (*F*) state. The Engelman scale was used during comparison and correlation coefficients were calculated with or without F336Y mutant data. The Pearson correlation in the basal state with F336Y is 0.9358; without F336Y, it is 0.9945. In the receptor-mediated state, the Pearson correlation with F336Y is 0.6992; without F336Y, it is 0.4861.

loop, we cross-linked α1 to α5 to minimize the disruption of its interactions with the guanine ring by translocation toward the receptor. Cross-linking was performed between I56C/T329C residues on a cysteine-depleted $G\alpha_{i1}$ ($G\alpha_{i1}$ HI) protein (Fig. 4*A*). Without cross-linking, $G\alpha_{i1}$ HI I56C/T329C showed higher basal nucleotide exchange rates compared with the $G\alpha_{i1}$ HI protein (Fig. 4*B*, *black bars*). Moreover, as expected, substitution of Phe-336 for Cys on $G\alpha_i$ HI I56C/T329C further increased the protein activity. After cross-linking, the nucleotide exchange rate of cross-linked $G\alpha_{i1}$ cross-linking HI I56C/T329C was decreased as compared with un-cross-linked proteins, demonstrating the stabilizing effect of the cross-linking. Substitution of F336C on cross-linked $G\alpha_{i1}$ HI I56C/T329C increased basal protein activation as compared with the un-cross-linked $G\alpha_{i1}$ HI I56C/T329C-F336C mutant (Fig. 4*B*, *black bars*). This indicates that perturbation of Phe-336 can trigger the activation mechanism without translocation of α5 toward the receptor and disruption of β6-α5 loop region.

Because receptor-mediated activation causes both a rotation of the α5 helix and an uncoiling of one turn of helix, we expected the cross-linked Gα would be resistant to receptor-mediated activation. This is indeed what was found in both cross-linked proteins (Fig. 4*B*, *gray bars*). This result might be caused by the reduced capability of cross-linked Gα to interact with either Gβγ subunits or the receptor. To test the first possibility, we measured the basal nucleotide exchange rates of Gα mutants in the presence or absence of Gβγ subunits (Fig. 4*C*). The results showed that basal nucleotide exchange rates

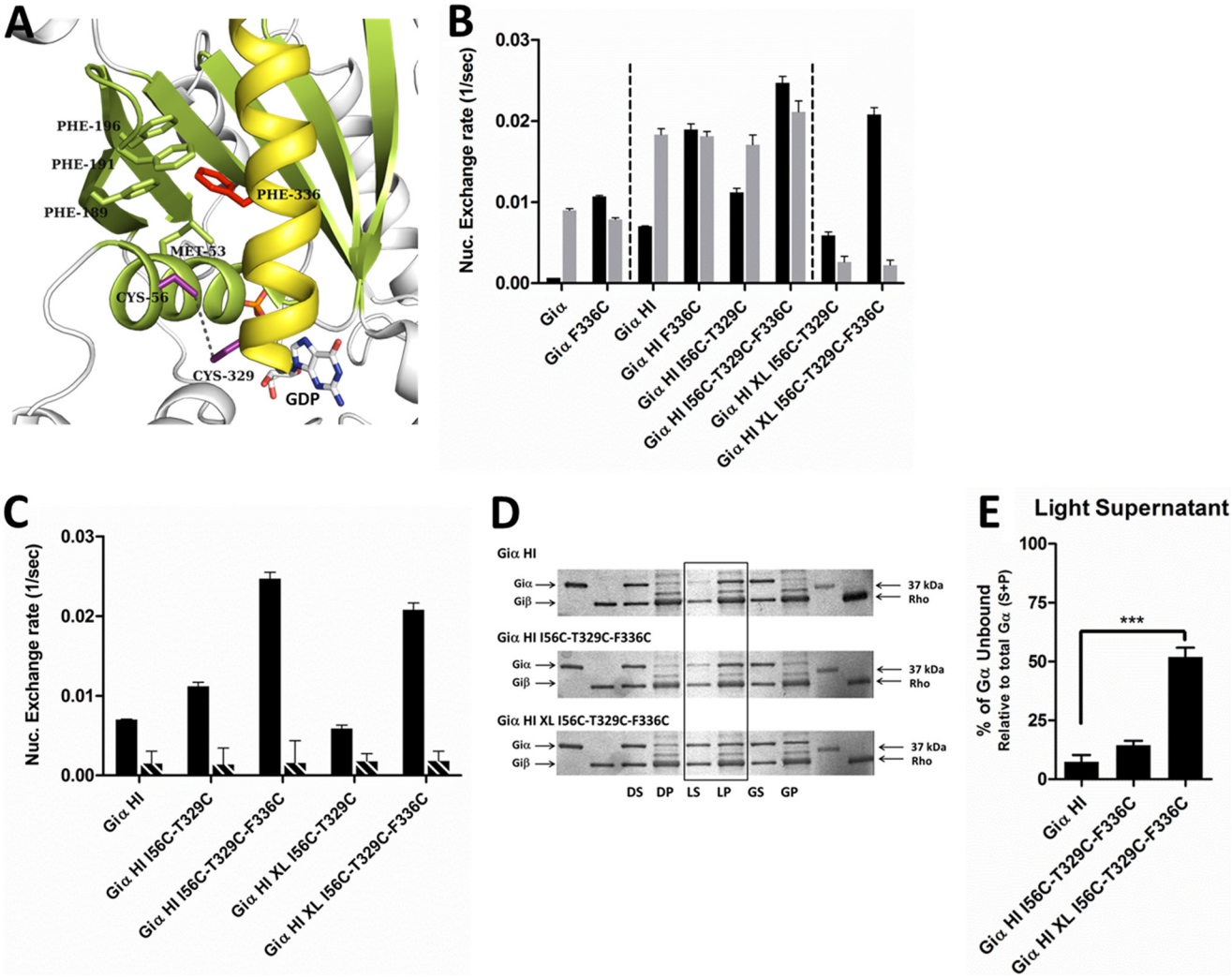

FIGURE 4. **Cross-linking of α1 and α5 helices of Gα1 HI.** *A*, cartoon representation of cross-linking region. Cross-linking was performed between I56C (α1) and T329C (α5) (*purple*) residues on a cysteine depleted $G\alpha_{i_1}$ ($G\alpha_{i_1}$ HI) protein. The Phe-336 (α5) residue is colored *red*, and the Phe-189 (β2), Phe-191 (β2), Phe-196 (β3), and Met-53 (α1) residues are colored *green*. The α5 helix is colored *yellow*, and the β1–β6 strands and α1 helix are colored *green*. *B*, basal (*black bars*) and receptor (*gray bars*) mediated nucleotide exchange rates for cross-linked $G\alpha_{i_1}$ HI proteins. *C*, basal nucleotide exchange rates in the presence of Gβγ subunit. *Black bars*, Gα; *striped bars*, Gαβγ. *D*, membrane binding of wild type and mutant $G\alpha_{i_1}$ HI proteins. Assay was performed as described under "Experimental Procedures." *DS*, supernatant from dark sample; *DP*, pellet fraction from dark sample; *LS*, supernatant from light sample; *LP*, pellet from light sample; *GS*, supernatant from light- and GTPγ*S*-activated sample; *GP*, pellet from light- and GTPγ*S*-activated sample; *XL*, cross-linked sample. *E*, densitometric quantification of supernatant from light samples. Each sample from SDS-PAGE (*D*) was evaluated by comparison of the amount of $G\alpha_{i_1}$ subunits in pellet (*P*) or supernatant (*S*) to the total amount of $G\alpha_{i_1}$ subunits ($P + S$) in both treatments and expressed as a percentage of the total $G\alpha_{i_1}$ protein. The data represent the averages of three independent experiments.

decreased on both cross-linked and un-cross-linked mutant Gα proteins in the presence of the Gβγ subunit, like the WT protein. This suggested that cross-linked Gα subunits were still capable of interacting with Gβγ subunits. To test the receptor binding capability of mutant $G\alpha_{i_1}$ subunits, we determined the effect of cross-linking on the membrane association of the G protein with light-activated rhodopsin, a measure of the formation of the high affinity receptor-G protein complex. As expected, cross-linking between α1 and α5 impaired this membrane binding (Fig. 4, *D* and *E*), consistent with a lack of ability of the cross-linked α5 helix to translocate toward the receptor and the decreased nucleotide exchange rates. Overall, the cross-linking data suggest that perturbation of Phe-336 triggers GDP release through destabilization of switch I-II regions via perturbing the α5 helix interactions along the α1 helix and β2-β3 strands rather than disrupting the β6-α5 loop region.

Hydrophobic Interactions around Phe-336: α1 Helix Interface Binding Energy and G Protein Activation—Previous data suggested that the interaction of Phe-336 with the α1 helix and β2-β3 strands might be crucial for domain opening because the α1 helix is positioned at the interface of the Gαi-GTPase domain and the helical domain (25). In addition, the α1 helix and β2-β3 strands interact with the phosphate binding loop and switch I-II, respectively. To probe the effects of hydrophobic interactions around Phe-336 with the α1 helix, we computed interaction energies for all residues within the α1 helix in both basal and receptor-bound states of the heterotrimeric Giαβγ using our established protocol (26). These $\Delta\Delta G$ values probed for a potential network of intramolecular interactions that could propagate the conformational changes necessary for G protein activation and nucleotide exchange. $\Delta\Delta G$ calculations predicted the importance of π-π interactions between the

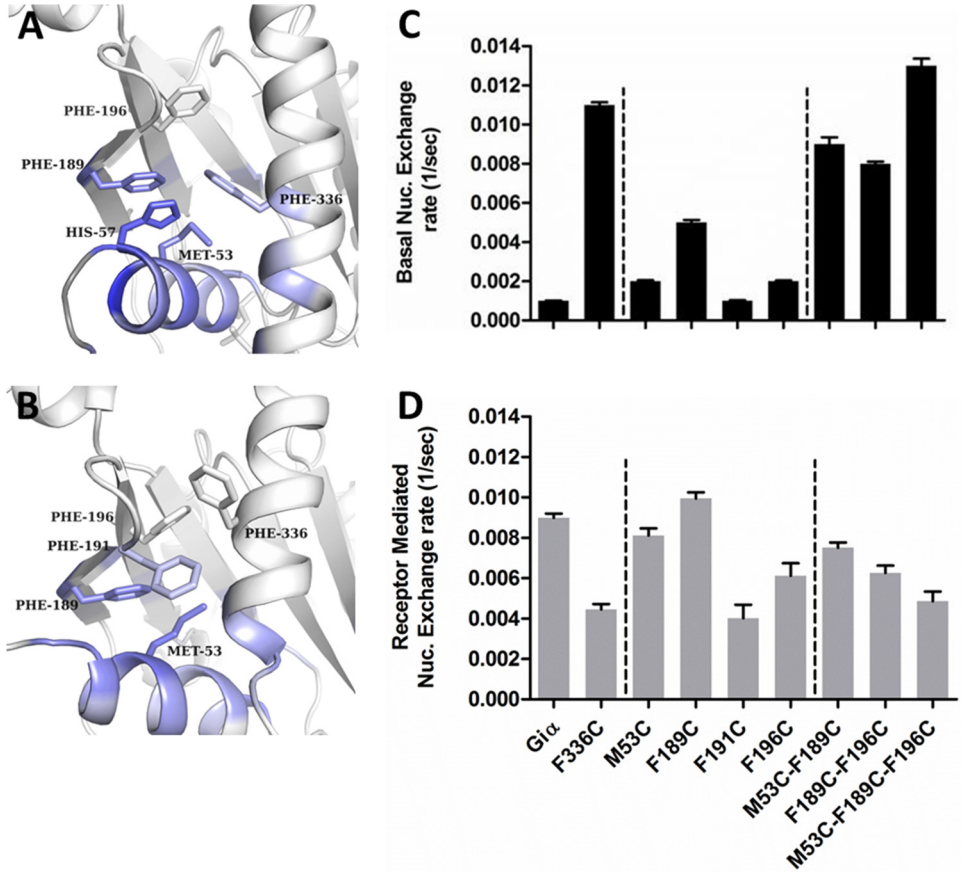

FIGURE 5. **The effects of hydrophobic residues around Phe-336 on nucleotide exchange rates.** *A* and *B*, Rosetta energetic analysis of the interface between α1 helix and GTPase domain in the basal state (*A*) and receptor-bound state (*B*). Residues are colored by the interaction energy in REU (*dark blue*, the most attractive). *C* and *D*, basal (*C*) and receptor-mediated (*D*) nucleotide exchange rates of single, double, and triple mutants within the β2-β3 strands and α1 helix as determined by monitoring intrinsic tryptophan (Trp-211) fluorescence changes upon addition of GTPγS. The data were collected at 21 °C for 45 min. The results represent the means ± S.E. values of at least three independent experiments.

aromatic rings of Phe-189 and His-57 in the β2 strand and α1 helix, respectively (Fig. 5*A* and Table 2). This pairwise interaction couples with Phe-336 on the α5 helix. Other predicted stabilizing interactions between α1 (Gln-52 and Ile-56) keep the α5 helix (Thr-329) fixed in the receptor unbound state; receptor interaction triggers unwinding of a turn of the α5 helix, disturbing this interaction (Fig. 5*B* and Table 2). On the face of α1, in contact with the helical domain, residues (Lys-51, Lys-54, Ile-55, Tyr-61, and Leu-175) on both the α1 and αF helices assist to secure the helical domain in a "closed" GDP-bound conformation. The total interaction energy was ~25.4 REU. In the basal state, the α1 helix was predicted to interact favorably with β2-β3 (Phe-189, Met-198, and Asp-200; 3.59 REU), α5 (Val-332 and Phe-336; REU 2.44), and helical domain (Glu-65 and Leu-175; 1.84 REU) (Table 2). In the receptor-bound state, the α1 helix was predicted to interact favorably with α5 (Asn-331 and Val-332; 2.1 REU), and as expected, the overall interaction was calculated as lower than the unbound state (Table 2).

To test our computational results, we mutated two residues that are predicted to stabilize the α1-α5 interaction (Phe-189 and Phe-191). In the basal state, F189C increased nucleotide exchange 5-fold, whereas F191C showed no change relative to WT $G\alpha_{i1}$ (Fig. 5*C*). We prepared double and triple mutants with M53C and F196C mutants, which we had previously tested (26). Double mutants (M53C/F189C and F189C/F196C) exhibited similar basal activation and a triple mutant (M53C/F189C/F196C) showed an even higher basal exchange rate compared with the F336C $G\alpha_{i1}$ mutant protein (Fig. 5*C*). In receptor-mediated activation of exchange, there was again a pattern of only modest inhibition, with F191C showing the largest decrease (Fig. 5*D*) consistent with previously predicted α5 (26) and α1 interface binding energy calculations.

Perturbation of Phosphate Site of Nucleotide Binding Region with Phe-336 Mutants—To determine whether the hydrophobic pocket around Phe-336 was necessary to control the local order of the phosphate binding region of GDP, we used the sensitive monitor of Mg^{2+} binding into this region. Three different strategies were used to investigate the influence of $G\alpha_{i1}$ mutants on Mg^{2+} binding to this region: (*a*) [Mg^{2+}] effects on the kinetics of nucleotide exchange, (*b*) AlF_4^- binding, and (*c*) trypsin digestion of $G\alpha_{i1}$ in the presence of different concentrations of Mg^{2+}. The results showed that the high nucleotide exchange rates of the mutants could be decreased in elevated Mg^{2+} concentrations (Fig. 6, *A* and *B*), suggesting that these mutations had allosteric effects on the phosphate binding region that could be overcome with higher Mg^{2+} concentration. The highest decrease in the rate of exchange, as a function of increasing concentrations of Mg^{2+}, was observed for the

TABLE 2
G protein α subunit α1 helix interface energetic prediction

Entity	Amino acid	Energy	Standard deviation	Z-score
		REU		
Free Gα				
β1	Leu-038	0.87	±0.04	22.75
α1	Lys-046	1.14	±0.28	4.01
α1	Ser-047	0.95	±0.04	21.55
α1	Thr-48	1.82	±0.05	38.27
α1	Ile-49	0.99	±0.09	11.42
α1	Lys-51	0.82	±0.1	8.10
α1	Gln-52	1.65	±0.05	34.32
α1	Met-53	1.33	±0.11	12.04
α1	Lys-54	2.49	±0.07	38.00
α1	Ile-5	1.03	±0.16	6.53
α1	Ile-56	1.07	±0.03	32.77
α1	His-57	1.73	±0.08	22.03
Helical	Glu-65	0.78	±0.11	6.96
Helical	Leu-175	1.06	±0.08	13.10
β2	Phe-189	1.41	±0.09	15.72
β3	Met-198	0.50	±0.12	4.28
β3	Asp-200	0.81	±0.33	2.45
β6-α5	Ala-326	1.62	±0.04	41.26
β6-α5	Thr-329	0.82	±0.02	41.22
α5	Val-332	0.85	±0.03	31.85
α5	Phe-336	0.72	±0.05	15.83
GDP		0.95	±0.13	7.32
GDP	Cumulative	0.95		
α1	Cumulative	15.02		
Helical	Cumulative	1.84		
β6-α5	Cumulative	2.44		
α5	Cumulative	1.57		
β-strands	Cumulative	3.59		
Overall	Cumulative	25.43		
Receptor-Gα complex				
β1	Leu-038	0.78	±0.16	4.85
β1	Gly-40	0.72	±0.34	2.12
α1	Lys-46	1.58	±0.41	3.88
α1	Ser-47	0.71	±0.14	5.01
α1	Ile-49	1.11	±0.1	10.77
α1	Val-50	0.75	±0.16	4.61
α1	Lys-51	0.52	±0.34	1.55
α1	Gln-52	1.08	±0.13	8.03
α1	Met-53	1.62	±0.15	10.72
α1	Lys-54	0.94	±0.45	2.11
α1	Ile-56	1.18	±0.2	5.85
α1	His-57	1.20	±0.57	2.12
β2	Phe-189	1.43	±0.17	8.56
β2	Phe-191	0.55	±0.08	6.60
α5	Asn-331	1.02	±0.04	23.43
α5	Val-332	0.68	±0.08	8.11
GDP		0.70	±0.19	3.79
GDP	Cumulative	0.70		
α1	Cumulative	10.69		
α5	Cumulative	1.70		
β-strands	Cumulative	3.48		
Overall	Cumulative	16.57		

F336Y mutant, which showed the fastest exchange rate in the presence of low Mg^{2+} concentrations (Fig. 3*C*).

To investigate the order of the Mg^{2+} binding region in the presence of GDP, the AlF_4^- binding assay was used. In this assay, changes in intrinsic tryptophan fluorescence rates of $G\alpha_{i1}$ were measured upon AlF_4^- addition in the presence of different $MgCl_2$ concentrations. Mg^{2+} is necessary for AlF_4^- binding and generation of the active or transition state. Thus, this assay reflects both AlF_4^- and Mg^{2+} coordination in that region without nucleotide exchange. All mutations showed destabilization effects that were overcome with increasing Mg^{2+} concentration. The EC_{50} for Mg^{2+} stabilization of AlF_4^- binding for F336M, F336C, F336A, and F336Y was increased by 1.4-, 2.1-, 2.8-, and 3.1-fold, respectively, over the WT $G\alpha_{i1}$ under the same experimental conditions (Fig. 6*C*). In addition to the α5 helix mutants, the M53C/F189C/F196C mutant also exhibited statistically significant increased EC_{50} (Fig. 6*C*).

The sensitivity of the $G\alpha_{i1}$ mutants to the trypsin digestion assay is a complementary assay to show the subtle changes in local order at the trypsin digestion site at Arg-208 in the presence of varying Mg^{2+} concentrations. After activation by either GDP-AlF_4^- or GTPγS, $G\alpha_{i1}$ yields a ~34-kDa fragment following trypsin digestion. All high nucleotide exchange mutants had reduced stability as assayed by decreased 34-kDa fragment in the presence of low Mg^{2+} concentrations compared with the WT $G\alpha_{i1}$ subunit (Fig. 6*D*).

Structural Features of the X-ray Structures of the F336C and F336Y Mutants—To probe the structural basis for the increased rates of nucleotide exchange observed in the Phe-336 mutants, the crystal structures of the F336C and F336Y variants of the $G\alpha_{i1}$ subunit were determined in both the GDP- and the GTPγS-bound states. The data collection and refinement statistics are summarized in Table 1. The mutations in the protein were confirmed by the crystal structure, where electron density at position 336 corresponded to either cysteine or tyrosine (Fig. 7, *A* and *B*). The structures of the GDP-bound form of F336C and F336Y $G\alpha_{i1}$ were refined to 2.0 and 2.4 Å resolution, respectively. Both GTPγS-bound structures were refined to a resolution of 2.0 Å. The GDP- and GTPγS-bound structures for F336C and F336Y were determined in space groups identical to those of the WT $G\alpha_{i1}$ structures. Neither mutant showed significant structural differences compared with WT $G\alpha_{i1}$. Even with the Phe-336 mutations in the α5 helix, the crystal structures showed the same localization and similar average *B* (temperature) factors around Phe-336 region relative to those of WT $G\alpha_{i1}$ structures (Fig. 7*C*). The effects of Phe-336 mutations on the β2-β3 strands and β2-β3 loop were minimal (Fig. 7, *D* and *E*). Overall, the root mean square deviations between WT $G\alpha_{i1}$-GDP with F336C and F336Y $G\alpha_{i1}$-GDP were 0.42 and 0.36 Å (310 Cα atoms aligned of 324 total), respectively, whereas they were 0.31 and 0.29 Å (304 Cα atoms aligned of 315) for their GTPγS-bound structures.

DISCUSSION

The α5 helix of the Gα subunit is a critical region for both the receptor-mediated and basal activity (1, 9, 14, 15, 18). It is encircled by hydrophobic interactions from six β strands (β1–β6) and the α1 helix (α1). In the current study, we tested residues around the α5 helix that we predicted as critical for the function of this helix during G protein activation in our previous studies. We highlight information flow within the G protein, starting from the α5 helix to the GDP binding site of Gα using biochemical, structural, and computational approaches.

Our previous study predicted that Phe-336 within the α5 helix is an important amino acid for both the active and inactive states (26), a finding consistent with other studies (14, 28). Mutation of this residue resulted in constitutive activity in both monomeric and heterotrimeric G proteins (14, 16, 29, 47). It is also known that in small GTPases, structural perturbation of that region through mutation causes increased guanine nucleotide turnover that can lead to several diseases, including Noonan, cardiofaciocutaneous, and Costello syndromes (47–49).

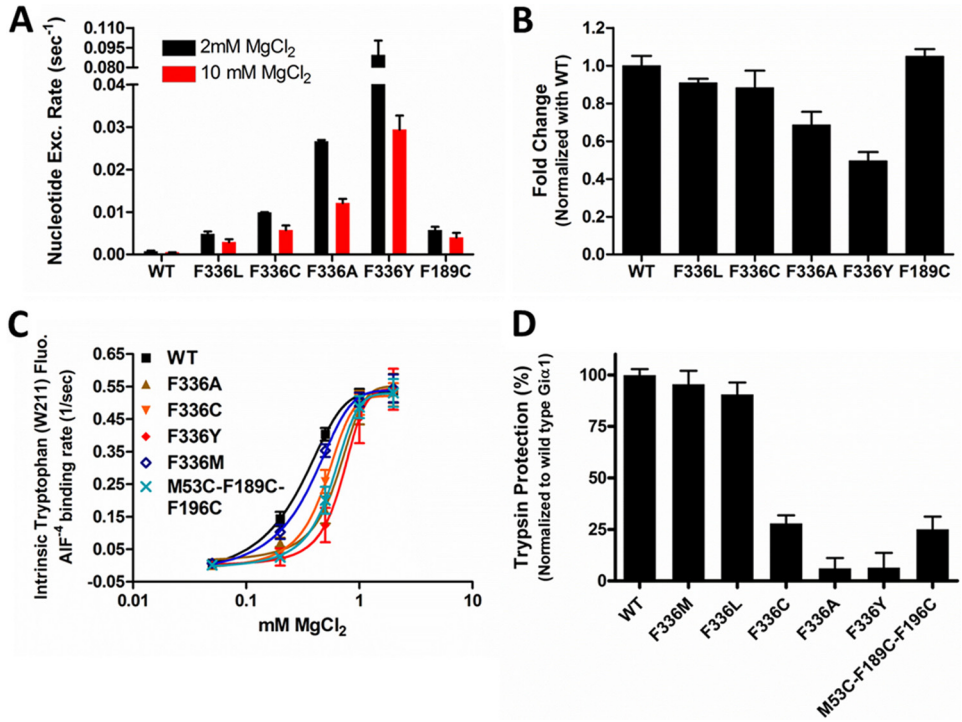

FIGURE 6. **The effect of $MgCl_2$ on $G\alpha_{i1}$ basal activity.** *A*, basal nucleotide exchange in the presence of 2 and 10 mM $MgCl_2$ concentrations. *B*, changes in the nucleotide exchange rate in the presence of different $MgCl_2$ concentrations. Fold change was calculated from *A* and normalized with $G\alpha_{i1}$ (WT) data. *C*, rates of intrinsic tryptophan fluorescence changes in $G\alpha_{i1}$ upon AlF_4^- addition in the presence of different $MgCl_2$ concentrations (0.1–2 mM). Intensity of tryptophan signal were monitored (excitation, 290 nm; emission, 340 nm) at 21 °C for 10 min before and after the addition of AlF_4^- (10 mM NaF and 50 μM $AlCl_3$). The data were calculated as described above and rate constants plotted against $MgCl_2$ concentrations. *D*, trypsin digestion and analysis of $G\alpha_{i1}$ protein subunit. The densitometric measurement of proteolytic fragments in the presence of GDP-AlF_4^- + 0.5 mM $MgCl_2$. The results were normalized with WT $G\alpha_{i1}$ data, and fragments were quantified by densitometry (Multimager; Bio-Rad). The results represent the means ± S.E. values of at least six to eight independent experiments.

In contrast to strong constitutive G protein activation, in this study, we did not observe drastic differences in the crystal structures of either GDP- or GTPγS-bound Phe-336 mutants. Like another highly constitutively active G protein mutant, $G\alpha_{i1}$ A326S (50), Phe-336 mutants showed similar structural features compared with WT $G\alpha_{i1}$. The guanine nucleotide provides a number of stabilizing interactions to the protein, perhaps inhibiting our ability to visualize subtle allosteric changes in the protein. In addition, other residues in the α5 helix and β-strands may contribute in holding this region intact during the crystallization process.

How does the perturbation at Phe-336 connect to the GDP binding region that is ~16 Å removed? Phe-336 is a part of a highly conserved hydrophobic core in the Gα subunit. The effect of Phe-336 mutations on basal G protein activation is correlated with the hydrophobicity of this region (Fig. 3, *C* and *E*). Once the receptor contacts the α5 helix and causes its rotation and displacement into the receptor binding site, this Phe-336 is now in a hydrophilic environment. We propose that breaking the hydrophobic core is a key event in perturbing GDP binding (26). Interestingly, we did not observe any effects of the hydrophilic mutants on receptor-mediated activation; this is likely due to the new solvent-exposed site, which prevents these side chains from contacting anything other than solvent upon receptor binding (Fig. 3, *D* and *F*).

To trace the hydrophobic interactions and to discern a possible interaction network from the Phe-336 residue to the GDP binding site, we computed binding energies of different regions in the Gα subunit by using different Rosetta algorithms. Adding to our previous calculations (α5 helix-$G_i\alpha$ interface binding energy (26)), we predicted that the Phe-336 side chain is mostly coupled with Met-53 (α1), Ile-56 (α1), Phe-189 (β2), Phe-191 (β2), Phe-196 (β3), Val-332 (α5), Gln-333 (α5), Val-339 (α5), and Thr-340 (α5). Thus, the effects of Phe-336 are not solely local and not coupled to a single residue but rather might be part of a distributed network of interactions in which the activation is coupled to changes in regions dispersed across both domains of the Gα subunit. Phe-336 is likely making direct hydrophobic contacts with Phe-191 and Met-53. It potentially communicates with Phe-189 via two paths.

The first is through residues Met-53, His-57, and Phe-191, which interact with Phe-189 through a π-π interaction between residues His-57 and Phe-189 (Fig. 5*A*). This is consistent with one of our previous studies (51) in which the constitutively active I56C(α1)/Q333C(α5) double mutant of $G\alpha_{i1}$ made a spontaneous disulfide bond between the α1 and α5 helices. This structure showed significant rearrangement of side chain residues His-57, Phe-189, Phe-191, and Phe-332 and disturbed π-π interaction between His-57 and Phe-189.

The second path begins from the direction of Phe-196, which interacts with Phe-336 via the Phe-191 and Thr-340 residues. These observations indicate that the perturbation effects of Phe-336 spread with complex interactions via the α1 helix and β2-β3 strands. These interactions also spread to the Mg^{2+} ion and the nucleotide binding region (Figs. 5 and 6) as evidenced by our nucleotide exchange data combined with the perturba-

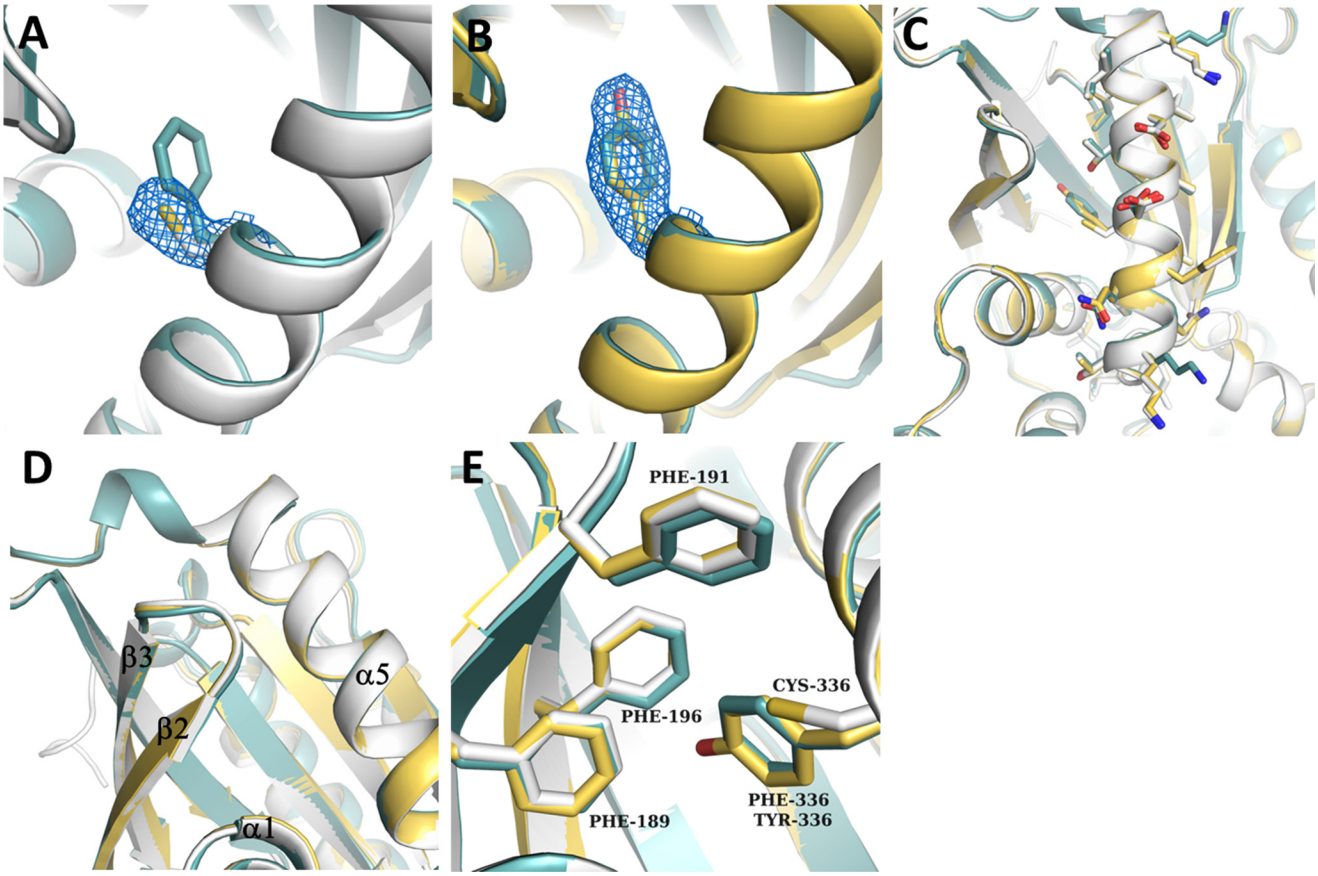

FIGURE 7. **Structural features of GDP bound Phe-336 mutant structures.** *A* and *B*, electron density for the F336C (*A*) and F336Y (*B*) side chains in the GDP bound state of $G\alpha_{i1}$. Corresponding regions in GDP-bound WT $G\alpha_{i1}$ (Protein Data Bank entry 1GDD (41); teal) are superposed. Difference electron density is from a $|F_o| - |F_c|$ omit map calculated after the removal of residues 330–340 and contoured to 3σ around the omitted side chain. *C*, comparison of the α5 helix between F336C-GDP (*white*), F336Y-GDP (*yellow*) and WT $G\alpha_{i1}$-GDP (Protein Data Bank entry 1GDD, *teal*). *D*, overview of the β2-β3 strands and β2-β3 loop. *E*, comparison of relative localization of Phe-189 (β2), Phe-191 (β2), Phe-196 (β3), and Phe-336 (α5) residues between F336C-GDP (*white*), F336Y-GDP (*yellow*), and WT-$G\alpha_{i1}$ (Protein Data Bank entry 1GDD, *teal*) structures.

tions seen in the Mg^{2+} and AlF_4^- assays, which supports previous studies (8, 16).

We also tested the effects of residues within the β5-β6 strands (Ile-265 (β5), Phe-267 (β5), Tyr-320 (β6), and His-322 (β6)) interacting with the other side of the α5 helix on G protein activation. We observed no major effects from the mutations either in the basal or receptor-mediated exchange assays. These data suggest how new interactions on the rotated α5 helix can compensate for the effects of single mutations in the β5 and β6 strands during receptor-mediated G protein activation. It also strongly suggests that the activation route goes through the other side of the protein (β1-β3/α1 to Switch I, phosphate binding loop, Mg^{2+} binding site, and GDP binding site), consistent with previously published findings (28). In addition, after restricting the C-terminal rotation and translocation by cross-linking the α1 and α5 helices, Phe-336 mutants can still induce increased basal nucleotide exchange (Fig. 4). This observation indicates that G proteins do not need a large displacement of α5 for basal state activation; rather, perturbing the β2-β3 and α1 regions are sufficient.

In summary, our study used a predictive energetic analysis to pinpoint information flow through Gα from receptor interaction to triggering of GDP release. We highlighted the hydrophobic interactions around Phe-336 as a key for stability of GDP binding, as well as removal of these hydrophobic interactions by receptor-mediated helical rotation to trigger GDP release. We suggested the route of information triggers through the α5 helix, β2-β3 strands, and the α1 helix using energetic analysis and mutagenesis. We also showed that the dynamics of the Mg^{2+} and β-phosphate binding area of GDP are perturbed by mutagenesis of this conserved residue. The β5-β6 residues that face the α5 helix are likely important structurally rather than functionally according to our analysis. Thus, our data suggest that after the initial interaction of the G protein with the receptor and C-terminal rotation, disruption of a conserved hydrophobic network around Phe-336 engages both β1-β3 and α1 to Switch I and the phosphate binding loop, which decreases the stability of the GDP binding pocket and triggers nucleotide release.

Acknowledgment—We thank Jin Liao for excellent technical assistance.

REFERENCES

1. Sprang, S. R. (1997) G Protein mechanisms: insights from structural analysis. *Annu. Rev. Biochem.* **66,** 639–678
2. Higashijima, T., Ferguson, K. M., Smigel, M. D., and Gilman, A. G. (1987) The effect of GTP and Mg^{2+} on the GTPase activity and the fluorescent

properties of G_o. *J. Biol. Chem.* **262,** 757–761
3. Oldham, W. M., and Hamm, H. E. (2007) How do receptors activate G proteins? *Adv. Protein Chem.* **74,** 67–93
4. Onrust, R., Herzmark, P., Chi, P., Garcia, P. D., Lichtarge, O., Kingsley, C., and Bourne, H. R. (1997) Receptor and βγ binding sites in the α subunit of the retinal G protein transducin. *Science* **275,** 381–384
5. Hamm, H. E. (1998) The many faces of G protein signaling. *J. Biol. Chem.* **273,** 669–672
6. Rasmussen, S. G., Choi, H. J., Rosenbaum, D. M., Kobilka, T. S., Thian, F. S., Edwards, P. C., Burghammer, M., Ratnala, V. R., Sanishvili, R., Fischetti, R. F., Schertler, G. F., Weis, W. I., and Kobilka, B. K. (2007) Crystal structure of the human β_2 adrenergic G-protein-coupled receptor. *Nature* **450,** 383–387
7. Rosenbaum, D. M., Rasmussen, S. G., and Kobilka, B. K. (2009) The structure and function of G-protein-coupled receptors. *Nature* **459,** 356–363
8. Scheerer, P., Park, J. H., Hildebrand, P. W., Kim, Y. J., Krauss, N., Choe, H. W., Hofmann, K. P., and Ernst, O. P. (2008) Crystal structure of opsin in its G-protein-interacting conformation. *Nature* **455,** 497–502
9. Oldham, W. M., Van Eps, N., Preininger, A. M., Hubbell, W. L., and Hamm, H. E. (2006) Mechanism of the receptor-catalyzed activation of heterotrimeric G proteins. *Nat. Struct. Mol. Biol.* **13,** 772–777
10. Okada, T., Fujiyoshi, Y., Silow, M., Navarro, J., Landau, E. M., and Shichida, Y. (2002) Functional role of internal water molecules in rhodopsin revealed by x-ray crystallography. *Proc. Natl. Acad. Sci. U.S.A.* **99,** 5982–5987
11. Ernst, O. P., Bieri, C., Vogel, H., and Hofmann, K. P. (2000) Intrinsic biophysical monitors of transducin activation: fluorescence, UV-visible spectroscopy, light scattering, and evanescent field techniques. *Methods Enzymol.* **315,** 471–489
12. Hamm, H. E., Deretic, D., Arendt, A., Hargrave, P. A., Koenig, B., and Hofmann, K. P. (1988) Site of G protein binding to rhodopsin mapped with synthetic peptides from the α subunit. *Science* **241,** 832–835
13. Palczewski, K., Kumasaka, T., Hori, T., Behnke, C. A., Motoshima, H., Fox, B. A., Le Trong, I., Teller, D. C., Okada, T., Stenkamp, R. E., Yamamoto, M., and Miyano, M. (2000) Crystal structure of rhodopsin: a G protein-coupled receptor. *Science* **289,** 739–745
14. Marin, E. P., Krishna, A. G., and Sakmar, T. P. (2001) Rapid activation of transducin by mutations distant from the nucleotide-binding site: evidence for a mechanistic model of receptor-catalyzed nucleotide exchange by G proteins. *J. Biol. Chem.* **276,** 27400–27405
15. Marin, E. P., Krishna, A. G., and Sakmar, T. P. (2002) Disruption of the α5 helix of transducin impairs rhodopsin-catalyzed nucleotide exchange. *Biochemistry* **41,** 6988–6994
16. Kapoor, N., Menon, S. T., Chauhan, R., Sachdev, P., and Sakmar, T. P. (2009) Structural evidence for a sequential release mechanism for activation of heterotrimeric G proteins. *J. Mol. Biol.* **393,** 882–897
17. Bourne, H. R. (1997) How receptors talk to trimeric G proteins. *Curr. Opin. Cell Biol.* **9,** 134–142
18. Rasmussen, S. G., DeVree, B. T., Zou, Y., Kruse, A. C., Chung, K. Y., Kobilka, T. S., Thian, F. S., Chae, P. S., Pardon, E., Calinski, D., Mathiesen, J. M., Shah, S. T., Lyons, J. A., Caffrey, M., Gellman, S. H., Steyaert, J., Skiniotis, G., Weis, W. I., Sunahara, R. K., and Kobilka, B. K. (2011) Crystal structure of the β_2 adrenergic receptor-G_s protein complex. *Nature* **477,** 549–555
19. Westfield, G. H., Rasmussen, S. G., Su, M., Dutta, S., DeVree, B. T., Chung, K. Y., Calinski, D., Velez-Ruiz, G., Oleskie, A. N., Pardon, E., Chae, P. S., Liu, T., Li, S., Woods, V. L., Jr., Steyaert, J., Kobilka, B. K., Sunahara, R. K., and Skiniotis, G. (2011) Structural flexibility of the $G\alpha_s$ α-helical domain in the β_2-adrenoceptor G_s complex. *Proc. Natl. Acad. Sci. U.S.A.* **108,** 16086–16091
20. Abdulaev, N. G., Ngo, T., Zhang, C., Dinh, A., Brabazon, D. M., Ridge, K. D., and Marino, J. P. (2005) Heterotrimeric G-protein α-subunit adopts a "preactivated" conformation when associated with βγ-subunits. *J. Biol. Chem.* **280,** 38071–38080
21. Oldham, W. M., Van Eps, N., Preininger, A. M., Hubbell, W. L., and Hamm, H. E. (2007) Mapping allosteric connections from the receptor to the nucleotide-binding pocket of heterotrimeric G proteins. *Proc. Natl. Acad. Sci. U.S.A.* **104,** 7927–7932
22. Iiri, T., Farfel, Z., and Bourne, H. R. (1998) G-protein diseases furnish a model for the turn-on switch. *Nature* **394,** 35–38
23. Cherfils, J., and Chabre, M. (2003) Activation of G-protein Gα subunits by receptors through Gα–Gβ and Gα–Gγ interactions. *Trends Biochem. Sci.* **28,** 13–17
24. Rondard, P., Iiri, T., Srinivasan, S., Meng, E., Fujita, T., and Bourne, H. R. (2001) Mutant G protein α subunit activated by Gβγ: a model for receptor activation? *Proc. Natl. Acad. Sci. U.S.A.* **98,** 6150–6155
25. Louet, M., Martinez, J., and Floquet, N. (2012) GDP release preferentially occurs on the phosphate side in heterotrimeric G-proteins. *PLoS Comput. Biol.* **8,** e1002595
26. Alexander, N. S., Preininger, A. M., Kaya, A. I., Stein, R. A., Hamm, H. E., and Meiler, J. (2014) Energetic analysis of the rhodopsin-G-protein complex links the α5 helix to GDP release. *Nat. Struct. Mol. Biol.* **21,** 56–63
27. Marin, E. P., Krishna, A. G., Archambault, V., Simuni, E., Fu, W. Y., and Sakmar, T. P. (2001) The function of interdomain interactions in controlling nucleotide exchange rates in transducin. *J. Biol. Chem.* **276,** 23873–23880
28. Ceruso, M. A., Periole, X., and Weinstein, H. (2004) Molecular dynamics simulations of transducin: interdomain and front to back communication in activation and nucleotide exchange. *J. Mol. Biol.* **338,** 469–481
29. Johnston, C. A., Willard, M. D., Kimple, A. J., Siderovski, D. P., and Willard, F. S. (2008) A sweet cycle for *Arabidopsis* G-proteins: recent discoveries and controversies in plant G-protein signal transduction. *Plant Signal. Behav.* **3,** 1067–1076
30. Mazzoni, M. R., Malinski, J. A., and Hamm, H. E. (1991) Structural analysis of rod GTP-binding protein, G_t: limited proteolytic digestion pattern of G_t with four proteases defines monoclonal antibody epitope. *J. Biol. Chem.* **266,** 14072–14081
31. Thaker, T. M., Kaya, A. I., Preininger, A. M., Hamm, H. E., and Iverson, T. M. (2012) Allosteric mechanisms of G protein-coupled receptor signaling: a structural perspective. *Methods Mol. Biol.* **796,** 133–174
32. Medkova, M., Preininger, A. M., Yu, N. J., Hubbell, W. L., and Hamm, H. E. (2002) Conformational changes in the amino-terminal helix of the G protein α_{i1} following dissociation from Gβγ subunit and activation. *Biochemistry* **41,** 9962–9972
33. Bradford, M. M. (1976) A rapid and sensitive method for the quantitation of microgram quantities of protein utilizing the principle of protein-dye binding. *Anal. Biochem.* **72,** 248–254
34. Coleman, D. E., and Sprang, S. R. (1998) Crystal structures of the G protein $G_i\alpha_1$ complexed with GDP and Mg^{2+}: a crystallographic titration experiment. *Biochemistry* **37,** 14376–14385
35. Schmidt, C. J., Thomas, T. C., Levine, M. A., and Neer, E. J. (1992) Specificity of G protein β and γ subunit interactions. *J. Biol. Chem.* **267,** 13807–13810
36. Linder, M. E., Middleton, P., Hepler, J. R., Taussig, R., Gilman, A. G., and Mumby, S. M. (1993) Lipid modifications of G proteins: α subunits are palmitoylated. *Proc. Natl. Acad. Sci. U.S.A.* **90,** 3675–3679
37. Van Eps, N., Preininger, A. M., Alexander, N., Kaya, A. I., Meier, S., Meiler, J., Hamm, H. E., and Hubbell, W. L. (2011) Interaction of a G protein with an activated receptor opens the interdomain interface in the α subunit. *Proc. Natl. Acad. Sci. U.S.A.* **108,** 9420–9424
38. Otwinowski, Z., and Minor, W. (1997) Processing of x-ray diffraction data collected in oscillation mode. In *Macromolecular Crystallography Part A* (Carter, C. W., Jr., and Sweet, R. M., eds) pp. 307–326, Academic Press, New York
39. Potterton, E., Briggs, P., Turkenburg, M., and Dodson, E. (2003) A graphical user interface to the CCP4 program suite. *Acta Crystallogr. D Biol. Crystallogr.* **59,** 1131–1137
40. Adams, P. D., Afonine, P. V., Bunkóczi, G., Chen, V. B., Davis, I. W., Echols, N., Headd, J. J., Hung, L.-W., Kapral, G. J., Grosse-Kunstleve, R. W., McCoy, A. J., Moriarty, N. W., Oeffner, R., Read, R. J., Richardson, D. C., Richardson, J. S., Terwilliger, T. C., and Zwart, P. H. (2010) PHENIX: a comprehensive Python-based system for macromolecular structure solution. *Acta Crystallogr. D Biol. Crystallogr.* **66,** 213–221
41. Mixon, M. B., Lee, E., Coleman, D. E., Berghuis, A. M., Gilman, A. G., and Sprang, S. R. (1995) Tertiary and quaternary structural changes in $G_i\alpha_1$ induced by GTP hydrolysis. *Science* **270,** 954–960

42. Coleman, D. E., Berghuis, A. M., Lee, E., Linder, M. E., Gilman, A. G., and Sprang, S. R. (1994) Structures of active conformations of $G_i\alpha_1$ and the mechanism of GTP hydrolysis. *Science* **265,** 1405–1412
43. Emsley, P., and Cowtan, K. (2004) Coot: model-building tools for molecular graphics. *Acta Crystallogr. D Biol. Crystallogr.* **60,** 2126–2132
44. Brünger, A. T., Adams, P. D., Clore, G. M., DeLano, W. L., Gros, P., Grosse-Kunstleve, R. W., Jiang, J. S., Kuszewski, J., Nilges, M., Pannu, N. S., Read, R. J., Rice, L. M., Simonson, T., and Warren, G. L. (1998) Crystallography & NMR system: A new software suite for macromolecular structure determination. *Acta Crystallogr. D Biol. Crystallogr.* **54,** 905–921
45. Winn, M. D., Ballard, C. C., Cowtan, K. D., Dodson, E. J., Emsley, P., Evans, P. R., Keegan, R. M., Krissinel, E. B., Leslie, A. G., McCoy, A., McNicholas, S. J., Murshudov, G. N., Pannu, N. S., Potterton, E. A., Powell, H. R., Read, R. J., Vagin, A., and Wilson, K. S. (2011) Overview of the CCP4 suite and current developments. *Acta Crystallogr. D Biol. Crystallogr.* **67,** 235–242
46. Krissinel, E., and Henrick, K. (2004) Secondary-structure matching (SSM), a new tool for fast protein structure alignment in three dimensions. *Acta Crystallogr. D Biol. Crystallogr.* **60,** 2256–2268
47. Quilliam, L. A., Zhong, S., Rabun, K. M., Carpenter, J. W., South, T. L., Der, C. J., and Campbell-Burk, S. (1995) Biological and structural characterization of a Ras transforming mutation at the phenylalanine-156 residue, which is conserved in all members of the Ras superfamily. *Proc. Natl. Acad. Sci. U.S.A.* **92,** 1272–1276
48. Søvik, O., Schubbert, S., Houge, G., Steine, S. J., Norgård, G., Engelsen, B., Njølstad, P. R., Shannon, K., and Molven, A. (2007) De novo HRAS and KRAS mutations in two siblings with short stature and neuro-cardio-facio-cutaneous features. *J. Med. Genet.* **44,** e84
49. Schubbert, S., Bollag, G., Lyubynska, N., Nguyen, H., Kratz, C. P., Zenker, M., Niemeyer, C. M., Molven, A., and Shannon, K. (2007) Biochemical and functional characterization of germ line KRAS mutations. *Mol. Cell. Biol.* **27,** 7765–7770
50. Posner, B. A., Mixon, M. B., Wall, M. A., Sprang, S. R., and Gilman, A. G. (1998) The A326S mutant of $G_i\alpha_1$ as an approximation of the receptor-bound state. *J. Biol. Chem.* **273,** 21752–21758
51. Preininger, A. M., Funk, M. A., Oldham, W. M., Meier, S. M., Johnston, C. A., Adhikary, S., Kimple, A. J., Siderovski, D. P., Hamm, H. E., and Iverson, T. M. (2009) Helix dipole movement and conformational variability contribute to allosteric GDP release in G_i subunits. *Biochemistry* **48,** 2630–2642
52. Oldham, W. M., and Hamm, H. E. (2006) Structural basis of function in heterotrimeric G proteins. *Q. Rev. Biophys.* **39,** 117–166
53. Chen, V. B., Arendall, W. B., 3rd, Headd, J. J., Keedy, D. A., Immormino, R. M., Kapral, G. J., Murray, L. W., Richardson, J. S., and Richardson, D. C. (2010) MolProbity: all-atom structure validation for macromolecular crystallography. *Acta Crystallogr. D Biol. Crystallogr.* **66,** 12–21